Neurogenetics
DOI 10.1007/s10048-012-0338-5

ORIGINAL ARTICLE

Late-onset Charcot–Marie–Tooth disease 4F caused by periaxin gene mutation

Shoko Tokunaga · Akihiro Hashiguchi · Akiko Yoshimura · Kengo Maeda · Takashi Suzuki · Hiroyo Haruki · Tomonori Nakamura · Yuji Okamoto · Hiroshi Takashima

Received: 26 June 2012 / Accepted: 4 July 2012

Abstract We identified the main features of Charcot–Marie–Tooth (CMT) disease, type 4F, caused by a periaxin gene (*PRX*) mutation in Japanese patients. Periaxin is known as one of the key myelination molecules, forming tight junction between myelin loop and axon. We collected 427 DNA samples from individuals with CMT or CMT-related neuropathy, negative for *PMP22* duplication. We investigated *PRX* mutations using a purpose-built resequencing array screen during the period 2006–2012. We detected two types of *PRX* mutations in three patients; one patient showed a novel homozygous p.D651N mutation and the other two showed homozygous p.R1070X mutation. All *PRX* mutations reported so far have been of nonsense or frameshift type. In this study, we found homozygous missense mutation p.D651N. Aspartate 651 is located in a repeat domain; its position might indicate an important function. *PRX* mutations usually lead to early-onset, autosomal-recessive demyelinating CMT neuropathy 4F (CMT4F) or Dejerine–Sottas disease; their clinical phenotypes are severe. In our three patients, the onset of the disease was at the age of 27 years or later, and their clinical phenotypes were milder compared with those reported in previous studies. We showed a variation of clinical phenotypes for CMT4F caused by a novel, nonsense *PRX* mutation.

Keywords Charcot–Marie–Tooth disease · Periaxin gene mutation · Adult onset · Demyelinating neuropathy

S. Tokunaga · A. Hashiguchi · A. Yoshimura · T. Nakamura · Y. Okamoto · H. Takashima
Department of Neurology and Geriatrics, Kagoshima University Graduate School of Medical and Dental Sciences,
Sakuragaoka 35-1,
Kagoshima City, Kagoshima 890-8520, Japan

K. Maeda
Department of Neurology,
National Hospital Organization Shiga Hospital,
Gochi 255,
Higashi-oumi City, Shiga 527-8505, Japan

T. Suzuki
Department of Neurology, Joetsu General Hospital,
Daidoufukuda 1-148,
Joetsu City, Niigata 943-8507, Japan

H. Haruki
Department of Neurology and Clinical Neuroscience,
Yamaguchi University Graduate School of Medicine,
Minamiogushi 1-1-1,
Ube City, Yamaguchi 755-0046, Japan

H. Takashima (✉)
Department of Neurology and Genetics, Kagoshima University Graduate School of Medical and Dental Sciences,
Sakuragaoka 8-35-1,
Kagoshima City, Kagoshima 890-8520, Japan
e-mail: thiroshi@m3.kufm.kagoshima-u.ac.jp

Introduction

Charcot–Marie–Tooth disease (CMT) is one of the most common inherited neurological disorders with peripheral neuropathies, with an estimated prevalence of 1 in 2,500 [1]. These progressive motor and sensory neuropathies include distal leg degeneration, pes cavus, hammer toes, and intrinsic muscle weakness and wasting. Electrophysiological or pathological studies are necessary for a proper diagnosis [2]. CMT incidents are usually classified as CMT1, the demyelinating form, or as CMT2, the axonal form, distinguished by nerve conduction velocities (NCV) of 38 m/s or less in the median nerve.

The periaxin gene (*PRX*) is located on chromosome 19 and encodes a protein involved in the maintenance of peripheral nerve myelin. *PRX* mutations cause early-onset demyelinating neuropathy, CMT4F, and Dejerine–Sottas

Published online: 01 August 2012

neuropathy [3, 4]. We extended the phenotypes associated with mutations in the *PRX* gene by the identification of two families with novel *PRX* mutations (C715X and R82fs) [5]. The patients with homozygous C715X mutation showed much more severe sensory than motor impairment and a relatively slow disease progression despite an early disease onset. In contrast, in case of the patient with homozygous R82fs mutation, the disease course was consistent with that of Dejerine–Sottas disease, with early onset, severe muscle weakness, and substantially diminished nerve conduction. Pathological analysis of sural nerve in patients in both families showed remarkable demyelination, onion bulb, and occasional tomacula formation with focal myelin thickening, abnormalities of the paranodal myelin loops, and focal absence of paranodal septate-like junctions between the terminal loops and axon [5]. Until date, 27 such patients have been reported, and most mutations were of nonsense or frameshift type [6].

In this study, we screened for *PRX* mutations in 427 CMT or CMT-related neuropathy patients and found three Japanese patients with *PRX* mutations. One of the three patients showed a homozygous missense mutation and two had nonsense mutations. We have described the clinical features of these CMT4F patients; all three patients showed an adult-onset, mild phenotype.

Materials and methods

Standard protocol approvals, registrations, and patient consent

All patients were referred by their primary physician or neurologist and had signed an informed consent forms approved by the Institutional Review Board of Kagoshima University.

We isolated DNA from the peripheral blood of each patient. Patients negative for *PMP22* (n=427) were selected and investigated for *PRX* mutations during the period 2006–2012. All patients showing demyelinating neuropathy were negative for CMT1A *PMP22* duplication, as shown by fluorescence in situ hybridization analysis. A total of 292 (192 American and 100 Japanese) control chromosomes were also examined.

Sural nerve biopsies, performed at the age of 40 years in patient 1 and 47 years in patient 3, were analyzed according to standard morphological procedures for light and electron microscopy.

Nerve conduction studies were performed using surface electrodes and percutaneous electrical stimulation. Motor nerve conduction studies (MNCS) were conducted on the median, ulnar, and tibial nerves. Sensory nerve conduction studies (SNCS) were performed on the median, ulnar, and sural nerves. We measured motor conduction velocity (MCV) and compound muscle action potential (CMAP) amplitude during the MNCS, and sensory conduction velocity (SCV) and sensory nerve action potential (SNAP) amplitude during the SNCS.

Genomic DNA was extracted from the peripheral blood leukocytes by conventional methods using the Gentra Puregene Blood Kit (Qiagen, Tokyo, Japan). A purpose-built GeneChip® CustomSeq® Custom Resequencing Array (Affymetrix, Santa Clara, CA) was designed to screen for CMT and related diseases such as ataxia with oculomotor apraxia type 1, ataxia with oculomotor apraxia type 2, spinocerebellar ataxia with axonal neuropathy type 1, and hereditary motor neuropathies. The designed resequencing array included the following 28 genes: *EGR2*, *PMP22*, *myelin protein zero* (*MPZ*), *gap junction protein beta 1*, *PRX*, *lipopolysaccharide-induced TNF factor*, *neurofilament light polypeptide* (*NEFL*), *ganglioside-induced differentiation associated protein 1* (*GDAP1*), *myotubularin-related protein 2*, *SH3 domain and tetratricopeptide*, *SET binding factor 2*, *N-myc downstream regulated 1*, *mitofusin 2*, *rab-protein 7*, *glycyl-tRNA synthetase*, *heat shock 27 kDa protein 1*, *heat shock 22 kDa protein 8*, *lamin A/C*, *dynamin 2*, *tyrosyl-tRNA synthetase*, *aranyl-tRNA synthetase*, *lysyl-tRNA synthetase*, *aprataxin*, *senataxin*, *tyrosyl-DNA phosphodiesterase 1*, *desert hedgehog*, *gigaxonin 1*, and *K-Cl cotransporter family 3*. We designed 363 primer sets to cover all coding exons and splice sites. The 363 polymerase chain reactions (PCRs) were amplified in 32 multiplex PCR reactions using the Qiagen Multiplex PCR system (Qiagen). Each reaction used 120 ng of genomic DNA, 10 pmol of the primer set, dNTP, and the Qiagen Multiplex PCR reaction mix (Qiagen). We generated each multiplex PCR product using the following conditions: 15 min at 95 °C, 42 cycles of amplification (94 °C for 30 s, 60 °C for 3 min, and 72 °C for 1 min 30 s), and 15 min at 68 °C. Pooling, DNA fragmentation, labeling, and chip hybridization were performed using the Affymetrix CustomSeq Resequencing protocol instructions [7]. The chips were washed in the Affymetrix Fluidics Station using CustomSeq Resequencing wash protocols. Analysis of microarray data was done using Gene Chip Sequence Analysis software v 4.0 (Affymetrix).

The mutations detected by our DNA Chip method were confirmed by conventional DNA Sanger sequencing. Briefly, we amplified 50 ng of genomic DNA using primers and the hot-start PCR method. Using a presequencing kit (USB, Cleveland, OH), we purified the patient PCR products detected by our resequencing array method and sequenced them with dye-primer chemistry using the ABI Prism 3130 Sequencer (Applied

Biosystems, Foster City, CA). We then aligned the resulting sequences and evaluated the mutations using the Sequencher sequence alignment program (Gene Codes, Ann Arbor, MI).

Results

Patient 1

This patient was a 65-year-old woman who was the third child of healthy, non-consanguineous parents. She had contracted infantile paralysis at the age of 18 months; as a result, her ability to walk independently was delayed. She noticed a mild distal lower limbs weakness and sensory impairment at the age of 30. Upper limbs wasting was observed at the age of 44 years and she also had vocal cord paralysis. The symptoms progressed very slowly. At the age of 65 years, a neurogenic examination revealed mild (upper proximal limbs), moderate (upper distal limbs and proximal lower limbs), and severe (distal lower limbs) muscle weakness, distal dominant sensory disturbance and areflexia. At that time, she had to use short leg braces and drive an electric wheelchair. Electrophysiological analysis showed that CMAPs and SNAPs were not detectable.

Patient 2

This patient was a 63-year-old woman who was the second child of healthy, non-consanguineous parents. At the age of around 50, she gradually acquired a mild wasting and a sensory disturbance in all extremities. At the age of 63 years, she had pes cavus and bilateral limb weakness, mild in upper and lower proximal limbs and moderate in lower distal limbs. Sensory examination showed a moderate reduction in touch and pinprick responses in hands and lower limbs. She could however walk without aid. Electrophysiology showed reduced MCV (20.5 m/s) in the median nerve.

Patient 3

This patient was a 47-year-old man who was the first child of healthy, non-consanguineous parents and had a younger healthy sister. His lower limbs weakness appeared at the age of 37 and progressed gradually. A neurological examination revealed moderate S-shaped scoliosis and severe lower motor impairment; his deep tendon reflexes were absent but he did not have pes cavus. At the age of 47 years, he could walk using a walking vehicle. Electrophysiological studies showed diminished motor NCVs and very prolonged distal latencies (Table 1).

Histopathology

Sural nerve biopsy was performed in patients 1, 2, and 3

Patient 1

Light microscopy indicated a significant loss of all types of fibers. When examined under electron microscope, Schwann cell projections were often scattered.

Patient 2

Light microscopy showed moderate loss of large myelinated fibers with onion bulb formations.

Patient 3

Light microscopy demonstrated a severe deficiency of both myelinated fibers. Many axons had onion bulb formations, but the remaining axons had thin myelin sheaths.

Genetic analysis

We tested each coding exon of *PRX* for mutations by DNA sequencing. Patient 1 carried a homozygous D651N mutation (Fig. 1a) and patients 2 and 3 were homozygous for R1070X mutation (Fig. 1b) [8]. The mutations D651N and R1070X were not found in 292 (192 American and 100 Japanese) control chromosomes or the chromosomes of 427 inherited neuropathy patients. However, we found a D651N mutation in the 1000-Genomes database cataloging human genetic variations using 1,197 samples (including 300 East Asian samples; http://browser.1000genomes.org). The analysis showed the allele frequency of 1 out of 2,188.

Discussion

Here, we report three patients with mutation. To our knowledge, 27 patients with *PRX* mutations have been described so far (Fig. 2) [3–5, 9–15]. All reported mutations were of nonsense or frameshift type. In this study, we report a patient with the homozygous missense mutation D651N.

Periaxin is a membrane-associated protein with a PDZ domain that is involved in mediating protein–protein interactions. Periaxin is mainly expressed in myelinating Schwann cells [18]. In adults, periaxin interacts with the dystroglycan complex (DGC) through dystrophin-related protein 2 and links the basal lamina to the Schwann cell cytoskeleton [19]. *Prx*-null mice develop grossly normal myelin fibers, however, cytoplasmic bands (Cajal bands) are disrupted and Schwann cell elongation during nerve

Table 1 Clinical, genetic, electrophysiological, and pathological characteristics of the patients

	Patient 1	Patient 2	Patient 3
Age (year)/gender	65/F	63/F	47/M
PRX mutation	D651N	R1070X	R1070X
Age of onset	28	50	37
Onset symptom	Muscle weakness in all distal limbs	Muscle weakness in all distal limbs	Muscle weakness in lower limbs
Pes cavus	(+)	(+)	(−)
Scoliosis	(−)	(−)	(+)
Hoarseness	(+)	(−)	(−)
Weakness UL	Distal, 3; proximal, 4	Distal, 4; proximal, 4	Distal, 4; proximal, 5
Weakness LL	Distal, 0; proximal, 3	Distal, 3; proximal, 4	Distal, 0; proximal, 2–4
Touch and pain sensation	Reduced in arms and legs	Reduced in hands and feet	Normal
Median nerve MCV (m/s)	NR	20.5	20.8
Median nerve CMAP amplitude (mv)	NR	0.67	0.7
Tibial nerve MCV (m/s)	NR	NR	NR
Tibial nerve CMAP amplitude (mv)	NR	NR	NR
Sural nerve SCV (m/s)	NR	42.2	NR
Sural nerve SNAP amplitude (μv)	NR	1.6	NR
Sural nerve biopsy	Significant demyelination	Moderate demyelination and complex onion bulbs	Thinning of the myelin sheaths and onion bulb

UL upper limbs, *LL* lower limbs, *MCV* motor conduction velocity, *CMAP* compound motor potentials, *SCV* sensory conduction velocity, *SNAP* sensory nerve action potential, *NR* not recordable

growth is impaired [20]. It is possible that unstable myelin structure causes CMT 4F loss of function in older animals [21]. Recently, it has been reported that laminin-2 and DGC are required for compartmentalization and elongation of the Schwann cell cytoplasm [22].

Most of the patients reported in the literature have first shown the CMT symptoms at the age of less than 7 years [6]. However, all our cases are of adult onset and have a milder phenotype; this information is important for the genetic diagnosis of CMT. In our study, two patients had a homozygous R1070X mutation. Some previous reports have described five patients in four families having R1070X alleles. R1070X mutation is relatively common in Japan [8, 11].

To the best of our knowledge, D651N mutation is the only reported missense mutation in *PRX*. We performed a sequence homology search by aligning protein sequences from several species using constraint-based multiple alignment tool (COBALT) (http://www.ncbi.nlm.nih.gov/tools/cobalt/) to identify pathogenicity of D651N mutation. Aspartate 651 was conserved among nine species analyzed (Fig. 3). Four species had glutamate instead of aspartate;

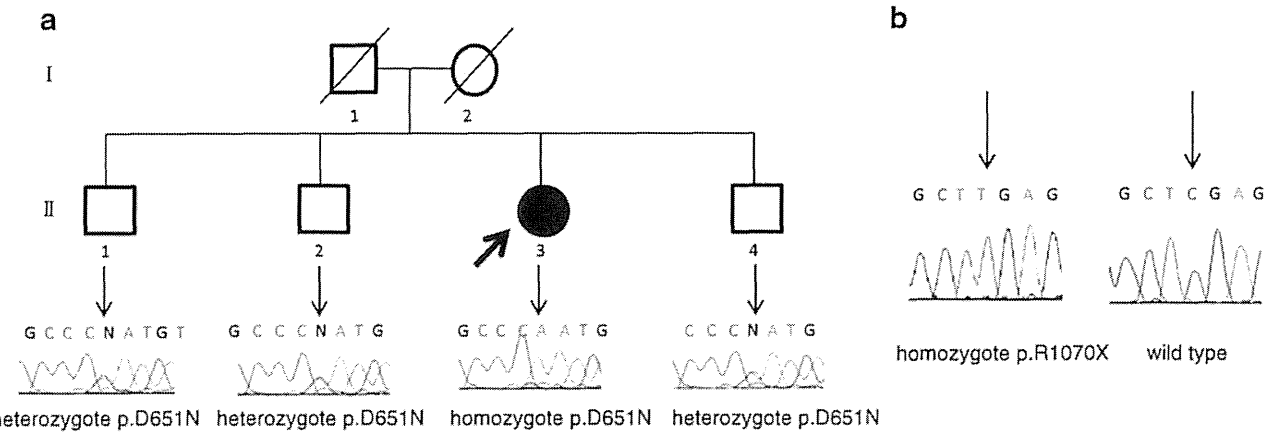

Fig. 1 **a** Chromatograms of *PRX* mutations identified in one family. *Filled symbol* indicates a patient with CMT. The DNA sequence chromatogram is shown below each symbol, with the specific mutation indicated by a *vertical arrow*. The CMT patient was homozygous, and her parents and unaffected brothers were heterozygous for D651N mutation. **b** Chromatograms with the homozygous C-to-T mutation (R1070X) and the wild-type sequence

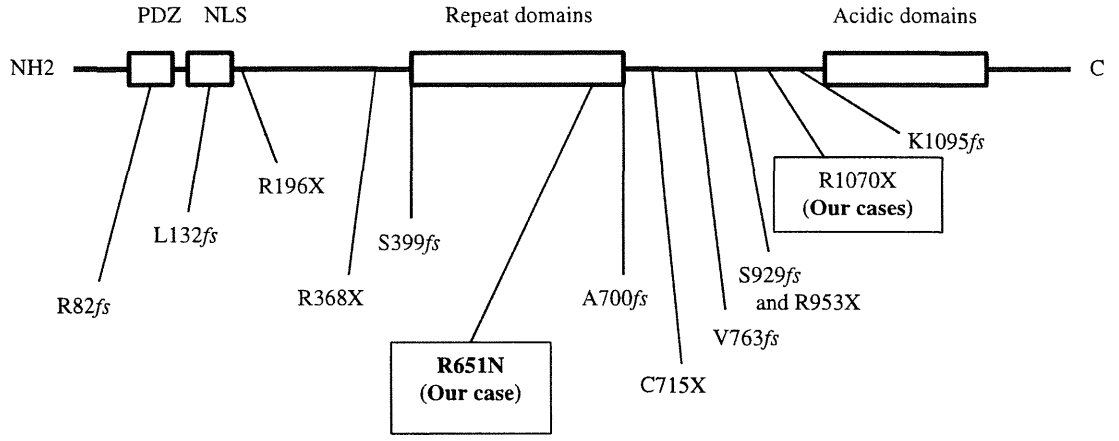

Fig. 2 The schema shows the location of previously reported *PRX* mutations and our novel mutation

aspartate and glutamate are very similar amino acids belonging to the same group with negatively charged side chains. Thus, the D651N mutation identified in a Japanese family was located in a well-conserved sequence of amino acids, suggesting that it might be a part of an important functional domain in *PRX*. Codon D651 is located in the repeat domain, which may have a triple peptide spacer of [LV]-P-[KER] which is known as a cornifin domain (UniProtKB; http://www.uniprot.org/uniprot/Q9BXM0). The cornifin family contains small proline-rich proteins that are strongly induced during the differentiation of human epidermal keratinocytes in vitro and in vivo [23]. Cornifins first appear in the cell cytosol, but ultimately become cross-linked to membrane proteins; they may also participate widely in the construction of cell envelopes [24]. Therefore, the potential mechanism of the periaxin mutation D651N is that it may lead to disruption of cytosol-membrane formation the Schwann cell. Taking into account the degree of conservation of the affected residues, D651N mutation is likely to be pathogen based. In addition, we computationally predicted the effect of D651N mutation on protein function using Sorting Intolerant From Tolerant (SIFT) (http://sift.jcvi.org/www/SIFT_enst_submit.html) algorithm; we obtained a score of 0.1 that indicates a pathogenic mutation. The algorithm uses evolutionarily conserved species as well as reference sequence alignments, physiochemical differences, and the proximity of various substitutions to predict functional domains and/or structural features. This D651N mutation was not detected in our 292 control alleles and only one heterozygous allele was found among 2,188 alleles in the 1000-Genomes database. To summarize, D651N mutation has a very low frequency, it segregates with the disease, the homozygous form of this mutation in the family has a positive score in SIFT, and it is conserved across species. These findings suggest that a homozygous D651N mutation could be the cause of CMT4F. We believe that the D651N mutation identified in our patients might affect periaxin function.

The electrophysiological and morphological analyses performed for the three patients gave results similar to those reported earlier, except that the disease had an adult onset.

Fig. 3 The homology analysis of periaxin in various species. Other vertebrates have aspartic acid or glutamic acid, but in our case there is a change from aspartic acid to aspartate. Repeat sequences highlighted in *gray* are relatively conserved across species

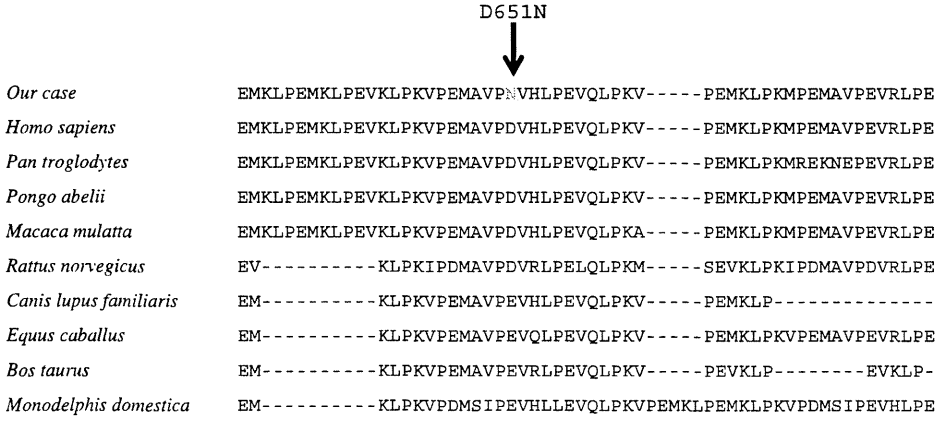

We propose that an adult-onset, demyelinating neuropathy unresponsive to immunotherapy could be caused by *PRX* mutation. Our analyses of the three patients confirmed the existence of putative loss-of-function mutations. One of the mutations was novel (D651N) and the other was the same as that previously observed (R1070X).

The vocal cord paralysis is well known in CMT disease 4A; it causes most frequent autosomal-recessive CMT form in the European and North American populations. The same symptom have been also reported for CMT 1, CMT 2C, CMT 2K, X-linked dominant CMT, and Dejerine–Sottas disease. The vocal cord paresis is a prominent feature in some types of CMT; GDAP1 mutations showed proximal muscle weakness, long history of the disease, and, frequently, a diaphragmatic involvement [16]. Another report on laryngeal neuropathy involving *PRX*, *NEFL*, and *MPZ* mutations demonstrated that the right vocal fold functions better than the left vocal fold [17]. Our cases had adult onsets, slowly progressing distal muscle weakness, normal respiration, and probably a restricted left vocal cord paralysis.

Until date, to the best of our knowledge, 12 pedigrees, carrying 13 mutations of *PRX* have been reported [6]. R1070X mutation has a high frequency among Japanese, but each R1070X is found in a different haplotype background. A Turkish patient with R1070X mutation has been also reported. Therefore, this mutation might be an ancestor allele in Japan or Asia, and is likely to be a hot-spot mutation [8].

Our adult-onset cases revealed that, clinically, D651N missense mutation shows a milder phenotype than that in previously reported cases. In adult patients with demyelinating neuropathies negative for CMT1A, we need to diagnose possible *PRX* mutation. However, as we have reported only a few cases, more research is needed to clarify which gene mutation is the most common in adult-onset CMT disease. Although we did not perform in vitro functional analysis of the D651N *PRX* mutation in this study, further functional studies should resolve the details of the pathomechanism of *PRX* mutations and the pathology of the missense mutation. Our observations add to a growing body of evidence that implicates specific genes/proteins in peripheral nerve function and delineates the pathological consequences of their dysfunction.

Acknowledgments We thank the families described in this report for their cooperation. This study was supported in part by grants from the Nervous and Mental Disorders and Research Committee for CMT Disease, Neuropathy, Ataxic Disease and Research on Applying Health Technology of the Japanese Ministry of Health, Welfare and Labour (H.T.)

Conflicts of interest H.T. has received the royalty for CMT genetic diagnosis *PRX* gene from Athena diagnostics.

References

1. Skre H (1974) Genetic and clinical aspects of Charcot–Marie–Tooth's disease. Clin Genet 6(2):98–118
2. Pareyson D, Marchesi C (2009) Diagnosis, natural history, and management of Charcot–Marie–Tooth's disease. Lancet Neurol 8 (7):654–667
3. Boerkoel CF, Takashima H, Stankiewicz P, Garcia CA, Leber SM, Rhee-Morris L, Lupski JR (2001) Periaxin mutations cause recessive Dejerine–Sottas neuropathy. Am J Hum Genet 68(2):325–333
4. Guilbot A, Williams A, Ravisé N, Verny C, Brice A, Sherman DL, Brophy PJ, LeGuern E, Delague V, Bareil C, Mégarbané A, Claustres M (2001) A mutation in periaxin is responsible for CMT4F, an autosomal recessive form of Charcot–Marie–Tooth disease. Hum Mol Genet 10(4):415–421
5. Takashima H, Boerkoel CF, De Jonghe P, Ceuterick C, Martin JJ, Voit T, Schröder JM, Williams A, Brophy PJ, Timmerman V, Lupski JR (2002) Periaxin mutations cause a broad sectrum of dymyelinating neuropathies. Ann Neurol 51:709–715
6. Marchesi C, Milani M, Morbin M, Cesani M, Lauria G, Scaioli V, Piccolo G, Fabrizi GM, Cavallaro T, Taroni F, Pareyson D (2010) Four novel cases of periaxin-related neuropathy and review of the literature. Neurology 75(20):1830–1838
7. Di X, Matsuzaki H, Webster TA, Hubbell E, Liu G, Dong S, Bartell D, Huang J, Chiles R, Yang G, Shen MM, Kulp D, Kennedy GC, Mei R, Jones KW, Cawley S (2005) Dynamic model based algorithms for screening and genotyping over 100 K SNPs on oligonucleotide microarrays. Bioinformatics 21(9):1958–1963
8. Otagiri T, Sugai K, Kijima K, Arai H, Sawaishi Y, Shimohata M, Hayasaka K (2006) Periaxine mutation in Japanese patients with Charcot–Marie–Tooth disease. J Hum Genet 51(7):625–628
9. Delague V, Bareil C, Tuffery S, Bouvagnet P, Chouery E, Koussa S, Maisonobe T, Loiselet J, Mégarbané A, Claustres M (2000) Mapping of a new locus for autosomal recessive demyelinating Charcot–Marie–Tooth disease to 19q13.1–13.3 in a large consanguineous Lebanese family: exclusion of MAG as a candidate gene. Am J Hum Genet 67(1):236–243
10. Banchs I, Casasnovas C, Albertí A, De Jorge L, Povedano M, Montero J, Martínez-Matos JA, Volpini V (2009) Diagnosis of Charcot–Marie–Tooth disease. J Biomed Biotechnol 2009:985415
11. Kijima K, Numakura C, Shirahata E, Sawaishi Y, Shimohata M, Igarashi S, Tanaka T, Hayasaka K (2004) Periaxin mutation cases early-onset but slow-progressive Charcot–Marie–Tooth disease. J Hum Genet 49(7):376–379
12. Parman Y, Battaloglu E, Baris I, Bilir B, Poyraz M, Bissar-Tadmouri N, Williams A, Ammar N, Nelis E, Timmerman V, De Jonghe P, Najafov A, Deymeer F, Serdaroglu P, Brophy PJ, Said G (2004) Clinicopathological and genetic study of early-onset demyelinating neuropathy. Brain 127:2540–2550
13. Kabzińska D, Drac H, Sherman DL, Kostera-Pruszczyk A, Brophy PJ, Kochanski A, Hausmanowa-Petrusewicz I (2006) Charcot–Marie–Tooth type 4F disease caused by S399fsX410 mutation in the PRX gene. Neurology 66(5):745–747
14. Auer-Grumbach M, Fischer C, Papić L, John E, Plecko B, Bittner RE, Bernert G, Pieber TR, Miltenberger G, Schwarz R, Windpassinger C, Grill F, Timmerman V, Speicher MR, Janecke AR (2008) Two novel mutations in the GDAP1 and PRX genes in early onset Charcot–Marie–Tooth syndrome. Neuropediatrics 39(1):33–38
15. Baránková L, Sisková D, Hühne K, Vyhnálková E, Sakmaryová I, Bojar M, Rautenstrauss B, Seeman P (2008) A 71-nucleotide deletion in the periaxin gene in a Romani patient with early-onset slow progressive demyelinating CMT. Eur J Neurol 15(6):548–551
16. Sevilla T, Jaijo T, Nauffal D, Collado D, Chumillas MJ, Vilchez JJ, Muelas N, Bataller L, Domenech R, Espinós C, Palau F (2008)

Vocal cord paresis and diaphragmatic dysfunction are severe and frequent symptoms of *GDAP1*-associated neuropathy. Brain 131 (11):3051–3061
17. Benson B, Sulica L, Guss J, Blitzer A (2010) Laryngeal neuropathy of Charcot–Marie–Tooth disease: further observations and novel mutations associated with vocal fold paresis. Laryngoscope 120(2):291–296
18. Dytrych L, Sherman DL, Gillespie CS, Brophy PJ (1998) Two PDZ domain proteins encoded by the murine periaxin gene are the result of alternative intron retention and are differentially targeted in Schwann cells. J Biol Chem 273(10):5794–5800
19. Sherman DL, Fabrizi C, Gillespie CS, Brophy PJ (2001) Specific disruption of a Schwann cell dystrophin-related protein complex in a demyelinating neuropathy. Neuron 30(3):677–687
20. Court FA, Sherman DL, Pratt T, Garry EM, Ribchester RR, Cottrell DF, Fleetwood-Walker SM, Brophy PJ (2004) Restricted growth of Schwann cells lacking Cajal bands slows conduction in myelinated nerves. Nature 431(7005):191–195
21. Gillespie CS, Sherman DL, Fleetwood-Walker SM, Cottrell DF, Tait S, Garry EM, Wallace VC, Ure J, Griffiths IR, Smith A, Brophy PJ (2000) Peripheral demyelination and neuropathic pain behavior in periaxin-deficient mice. Neuron 26(2):523–531
22. Court FA, Hewitt JE, Davies K, Patton BL, Uncini A, Wrabetz L, Feltri ML (2009) A laminin-2, dystroglycan, utrophin axis is required for compartmentalization and elongation of myelin segments. J Neurosci 29(12):3908–3939
23. Gibbs S, Fijneman R, Wiegant J, van Kessel AG, van De Putte P, Genomics BC (1993) Molecular characterization and evolution of the SPRR family of keratinocyte differentiation markers encoding small proline-rich proteins. Genomics 16(3):630–637
24. Hohl D, de Viragh PA, Amiguet-Barras F, Gibbs S, Backendorf C, Huber M (1995) The small proline-rich proteins constitute a multigene family of differentially regulated cornified cell envelope precursor proteins. J Invest Dermatol 104(6):902–909

Journal of the Peripheral Nervous System 17:206–209 (2012)

CASE REPORT

A novel *EGR2* mutation within a family with a mild demyelinating form of Charcot-Marie-Tooth disease

Kensuke Shiga[1], Yuichi Noto[1], Ikuko Mizuta[1], Akihiro Hashiguchi[2], Hiroshi Takashima[2], and Masanori Nakagawa[1]

[1] *Department of Neurology, Kyoto Prefectural University of Medicine, Graduate School of Medicine, Kyoto and* [2] *Department of Neurology and Geriatrics, Kagoshima University, Graduate School of Medical and Dental Sciences, Kagoshima, Japan*

Abstract Mutations of the early growth response 2 (*EGR2*) gene have been reported in a variety of severe demyelinating neuropathies such as autosomal recessive congenital hypomyelinating neuropathy, autosomal dominant child-onset Dejerine-Sottas neuropathy, and autosomal dominant adult-onset Charcot-Marie-Tooth disease (CMT). Here, we report on a heterozygous mutation in *EGR2* (c.1160C>A), which results in threonine at position 387 being changed to asparagine, in a family with a mild demyelinating form of adult-onset CMT. Of note, both the proband and her asymptomatic son exhibited neither pes cavus nor champagne-bottle leg atrophy, suggesting that the heterozygous T387N mutation may result in a relatively mild phenotype of demyelinating CMT.

Key words: Charcot-Marie-Tooth disease, demyelinating neuropathy, *EGR2* mutation, heterozygous mutation, mild phenotype

Introduction

Subtype of CMT and associated gene mutation

This case report chronicles a family with autosomal dominant demyelinating Charcot-Marie-Tooth disease (CMT) and mutations in the early response 2 gene (*EGR2*) (CMT1D, OMIM 607678).

Description of the case

The proband was a 46-year-old woman who had been healthy until 2 years ago, when she noticed a subtle tingling sensation on the dorsal aspect of her left hand. One year later, she started to have difficulty screwing off bottle caps and visited our facility. The proband was the only daughter of a father who died due to gastric cancer at 59 years of age and a mother who died due to diabetes at 63 years of age; neither parent had neuromuscular disease, but the mother was known to be a slow runner. The patient had three sons: the eldest was a 24-year-old part-time worker, the second was a 19-year-old office worker, and the youngest was a 16-year-old high school student. All of them were able to run, but the second son was a slow runner when he was a student.

Neurological examination of the proband revealed that the cranial nerves were normal. The left thenar prominence showed mild atrophy; however, neither hammer toes nor pes cavus were noticed. The Medical Research Council (MRC) scores were 4 in the abductor pollicis brevis, tibialis anterior, and extensor hallucis longus muscles, and 5 in the other muscles. Sensations were preserved except for subtle paresthesias on the dorsal aspect of her left hand. Both patellar tendon reflexes and Achilles tendon reflexes were absent, whereas reflexes were preserved in the upper extremities.

The results of nerve conduction studies (NCS) of the proband are shown in Table 1. Distal motor

Address correspondence to: Kensuke Shiga, MD, Department of Neurology, Kyoto Prefectural University of Medicine, Graduate School of Medicine, Kajiicho 465, Kamigyo-ku, Kyoto 602-8566, Japan. Tel: +81-75-251-5793; Fax: +81-75-211-8645; E-mail: kenshiga@koto.kpu-m.ac.jp

Table 1. Results of the motor nerve conduction and sensory nerve conduction studies in the proband.

	Median nerve, right	Ulnar nerve, right	Tibial nerve, right
Motor nerve conduction study			
Distal latency (ms)	5.96	4.12	6.72
CMAP (mV)	7.33	10.18	7.28
Duration (ms)	6.16	6.14	7.36
MCV (m/s), distal segments	24.0	28.9	23.2
MCV (m/s), proximal segments	26.1	25.9	—
Sensory nerve conduction study			
SNAP (μV)	1.3	0.9	Not evoked
SCV (m/s)	29.6	32.9	—

The distal median nerve MCV was measured between the wrist and elbow, whereas the proximal median nerve MCV was measured between the elbow and axilla. The distal ulnar nerve MCV was measured between the wrist and below the elbow and the proximal ulnar nerve MCV was measured below and above the elbow. The tibial nerve MCV was measured between the ankle and popliteal fossa. SCVs were measured between the wrist and the index and between the wrist and little fingers in the median and ulnar nerves, respectively, and between the LM and the distal shin 14 cm proximal to the LM.
CMAP, compound muscle action potential; LM, lateral malleolus; MCV, motor conduction velocity; SCV, sensory conduction velocity; SNAP, sensory nerve action potential.

latencies were prolonged in the median, ulnar, and tibial nerves. The motor nerve conduction velocities (MCVs) of these nerves were decreased equally in both the distal and proximal segments and the electric thresholds were markedly increased elsewhere. On the other hand, the compound muscle action potentials were relatively preserved. In the sensory NCS, sensory nerve action potentials (SNAPs) were markedly reduced or were not elicitable. The symmetric and uniform slowing of MCVs in a length-dependent manner suggested dysmyelination, the developmental defect in myelination, favoring a diagnosis of CMT1 (demyelinating form).

After obtaining a written informed consent from the patient, DNA was extracted from the proband's lymphocytes and was subjected to fluorescence *in situ* hybridization analysis for peripheral myelin protein (*PMP22*) duplication. Results showed the presence of the normal two copies of the gene. DNA was then analyzed further using a custom-built GeneChip® CustomSeq® Resequencing Array (Affimetrix, Santa Clara, CA, USA). This array was designed to screen for the following 28 CMT-related genes: *PMP22, myelin protein zero* (*MPZ*), *gap junction protein beta 1* (*GJB1*), *EGR2, periaxin* (*PRX*), *lipopolysaccharide-induced TNF factor* (*LITAF*), *neurofilament light chain* (*NEFL*), *ganglioside-induced differentiation association protein 1* (*GDAP1*), *myotubularin-related protein 2* (*MTMR2*), *SH3 domain and tetratricopeptide repeats 2* (*SH3TC2*), *SET-binding factor 2* (*SBF2*), *N-myc downstream regulated 1* (*NDRG1*), *mitofusin 2* (*MFN2*), *rab-protein 7* (*RAB7*), *glycyl-tRNA synthetase* (*GARS*), *heat shock 27 kDa protein 1* (*HSPB1*), *heat shock 22 kDa protein 8* (*HSPB8*), *lamin A/C* (*LMNA*), *dynamin 2* (*DNM2*), *tyrosyl-tRNA synthetase* (*YARS*), *alanyl-tRNA synthetase* (*AARS*), *lysyl-tRNA synthetase* (*KARS*), *aprataxin* (*APTX*), *senataxin* (*SETX*), *tyrosyl-DNA phosphodiesterase 1* (*TDP1*), *desert hedgehog* (*DHH*), *gigaxonin 1* (*GAN1*), and *K-Cl cotransporter family 2* (*KCC3*). The technical details of the array have been described in another publication *(Nakamura et al., 2012)*. The authors had obtained the approval of the genetic analysis using GeneChip from the institutional review boards of both institutions (Kyoto Prefectural University of Medicine and University of Kagoshima). The results showed a novel heterozygous mutation in *EGR2* (c.1160C>A) resulting in change of threonine at position 387 to asparagine (Fig. 1). To elucidate the pathogenicity of this mutation, we performed familial segregation analysis. The proband and all her sons agreed to participate in the study on written informed consent. Neurological examination of the second son unexpectedly revealed mild weakness of the extensor hallucis longus and tibialis anterior muscles, with an MRC score of 4. In addition, he had diminished patellar and Achilles tendon reflexes. In contrast, the eldest and youngest sons had normal neurological examination findings. The results of NCS for the right median nerve of the proband and her three sons are shown in Table 2. The median MCVs were decreased to 21.5 and 19.5 m/s in the proband and her second son, respectively, whereas those of the eldest and youngest sons were within the normal range. In addition, median SNAPs and sensory conduction velocities were also decreased in the proband and her second son, but remained normal in the other sons. The direct sequencing of *EGR2* revealed a heterozygous c.1160C>A mutation in the second son and a homozygous wild-type sequence in the other sons (Fig. 1). In summary, the heterozygous mutation of *EGR2* (c.1160C>A) was associated with a mild demyelinating neuropathy phenotype in this family.

Discussion

EGR2 is a "master" transcription factor that regulates myelination of the peripheral nervous system and plays a role in the maintenance of myelin *(Topilko et al., 1994; Warner et al., 1998)*. Genetic alteration of *EGR2* results in a variety of relatively severe demyelinating neuropathies such as congenital hypomyelinating neuropathy *(Warner et al., 1998)*, childhood-onset Dejerine-Sottas neuropathy (DSN)

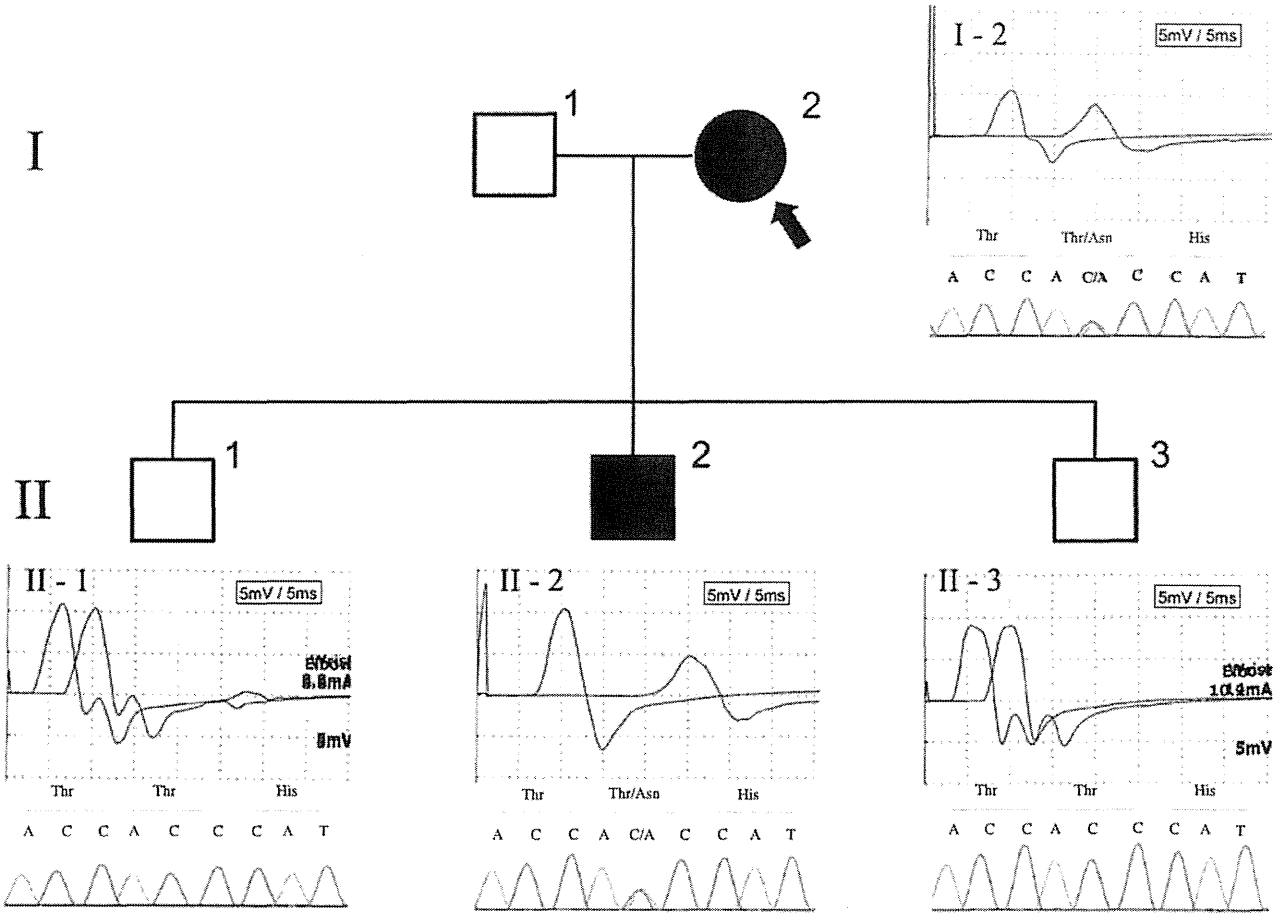

Figure 1. Family segregation study. I-2 (closed arrow): the proband, II-1: eldest son, II-2: second son, III-3: youngest son. Compound muscle action potentials (CMAPs) elicited by supramaximal stimulation of the right median nerve at the wrist and elbow were obtained for each family member, and these CMAPs were superimposed on each other. The onset of CMAPs was delayed in both I-2 and II-2. The chromatograms of the direct sequencing of exon 2 of early response 2 gene (*EGR2*) are shown below. A heterozygous c.1160C>A mutation was noted in both I-2 and II-2.

Table 2. Motor nerve and sensory nerve conductions in the median nerve of the proband and her sons.

Family member	I-2	II-1	II-2	II-3
Motor nerve conduction				
Distal latency (ms) (<4.2)	6.6	2.8	6.7	3.0
CMAP (mV) (>3.5)	5.4	10.7	10.4	8.9
MCV* (m/s) (>48)	21.5	56.1	19.0	57.6
Sensory nerve conduction				
SNAP (μV) (>19)	1.1	43.3	1.8	30.8
SCV† (m/s) (>47)	25.2	62.0	25.4	55.6

CMAP, compound muscle action potential; I-2 (closed arrow in Fig. 1), the proband; II-1, eldest son; II-2, second son; III-3, youngest son; MCV, motor conduction velocity; SCV, sensory conduction velocity; SNAP, sensory nerve action potential.
*MCVs were measured between the wrist and elbow.
†SCVs were measured between the wrist and index finger in the median nerves.

(Boekoel et al., 2001; Numakura et al., 2003; Szigeti et al., 2007), and adult-onset CMT type 1 *(Warner et al., 1998; Bellone et al., 1999; Yoshihara et al., 2001; Vandenberghe et al., 2002; Mikesová et al., 2005)*. In contrast, the proband in this report exhibited a rather milder phenotype, without typical features of CMT, such as champagne-bottle leg atrophy or pes cavus.

We consider c.1160C>A (p. Thr387Asn) in *EGR2* in the proband to be pathogenic for the following reasons. First, the amino acid alteration was clearly segregated in this family both with the reduced MCVs and with the mild neuropathic phenotype. Second, the nucleotide variation (c.1160C>A) has not been reported either in the dbSNP database or in the 1,000 genome catalog (as of January 2012). Third, the 387th amino acid threonine, located in the second zinc-finger domain of the EGR2 protein, is well conserved among different species ranging from humans to zebra fish. We thus assume that this amino acid alteration can affect the DNA-binding capacity of the protein transcription factor, possibly leading to

a defect in the myelinating process of Schwann cells. Finally, we computationally predicted the effect of p.Thr387Asn (T387N) on protein function using two distinct pathogenicity prediction algorithms: PolyPhen-2 (http://genetics.bwh.harvard.edu/pph2/) and MutationTaster (www.mutationtaster.org). Both programs predicted that T387N is most likely damaging or pathogenic (data not shown). The results of the segregation studies, conservation of T387 in a variety of species, and results of the two prediction algorithms point to the pathogenicity of T387N, presumably resulting in the demyelinating neuropathy.

Up to thirteen *EGR2* mutations have been reported to date in demyelinating neuropathies, most of which have early-onset or severe phenotypes. For instance, patients with D355V, R359W, R358Q, R381H, and R409W exhibit a child-onset CMT1 phenotype, whereas patients with R381H and G412V exhibit DSN. While nine patients exhibited severe childhood-onset CMT or DSN/CHN, one patient with R381C presented with an adult-onset mild CMT1 phenotype at 59 years of age. Similar to the case presented in this report, the patient with R381C also exhibited a mild demyelinating phenotype without atrophy of the tibialis anterior muscle. The clinical findings in the proband can be explained, in part, by a weak pathogenicity T387N mutation, possibly because both threonine and asparagine are hydrophilic polarized amino acids, and thus, the mutation resulted only in mild functional loss of EGR2.

Recognition of the mild CMT phenotype can be critical for two reasons. First, some patients with CMT disease with atypical presentations, such as asymmetric symptoms, can be misdiagnosed as having chronic inflammatory demyelinating polyradiculoneuropathy (CIDP) and may be treated with unnecessary and costly therapeutic interventions such as immunoglobulin administration. Second, recognition of CMT can prevent the administration of potentially risky neurotoxic drugs, for example, vincristine, which can be toxic in the demyelinating form of CMT *(Weiss et al., 1974)*. This form of CMT has recently been found in another patient with an *EGR2* mutation *(Nakamura et al., 2012)*. Therefore, we consider that early recognition and diagnosis of CMT is crucial, even if the patient presents with a mild phenotype as in this case.

Acknowledgements

This work was supported in part by Grants-in-Aid from the Research Committee of Charcot-Marie-Tooth Disease and the Research Committee of Neuropathy, Ataxic Disease and Applying Health and Technology, both of which were funded by the Ministry of Health, Labour, and Welfare of Japan. The funders had no role in the study design, data collection, analysis, decision to publish, or preparation of the manuscript.

References

Bellone E, Di Maria E, Soriani S, Varese A, Doria LL, Ajimar F, Mandich P (1999). A novel mutation (D305V) in the early growth response gene 2 is associated with severe Charcot-Marie-Tooth type 1 disease. Hum Mutat 14:353–354.

Boekoel CF, Takashima H, Bacino CA, Daenti D, Lupski JR (2001). EGR2 mutation R 359W causes a spectrum of Dejerine-Sottas neuropathy. Neurogenetics 3:153–157.

Mikesová E, Hühne K, Rautenstrauss B, Mazanec R, Baránková L, Vyhnálek M, Horácek O, Seeman P (2005). Novel EGR2 mutation R359Q is associated with CMT type 1 and progressive scoliosis. Neuromuscul Disord 15:764–767.

Nakamura T, Hashiguchi A, Suzuki S, Uozumi K, Tokunaga S, Takashima H (2012). Vicristine exacerbates asymptomatic Charcot-Marie-Tooth disease with a novel EGR2 mutation. Neurogenetics 13:77–82.

Numakura C, Shirahata E, Yamashita S, Kanai M, Kijima K, Matsuki T, Hayasaka K (2003). Screening of the early growth response 2 gene in Japanese patients with Charcot-Marie-Tooth disease type 1. J Neurol Sci 210:61–64.

Szigeti K, Wiszniewski W, Saifi GM, Sherman DL, Sule N, Adesina AM, Mancias P, Papasozomenos SC, Miller G, Keppen L, Daentl D, Brophy PJ, Lupski JR (2007). Functional, histopathologic and natural history study of neuropathy associated with EGR2 mutations. Neurogenetics 8:257–262.

Toplko P, Schneider-Maunoury S, Levi G, Baron-Van Evercooren A, Chennoufi AB, Seitanidou T, Charnay P (1994). Krox-20 controls myelination in the peripheral nervous system. Nature 371:796–799.

Vandenberghe N, Upadhyaya M, Gatignol A, Boutrand L, Boucherat M, Chazot G, Vandenberghe A, Latour P (2002). Frequency of mutations in the early growth response 2 gene associated with peripheral demyelinating neuropathies. J Med Genet 39:e81.

Warner LE, Mancias P, Butler IJ, McDonald CM, Keppen L, Koob G, Lupski JR (1998). Mutations in the early growth response 2 (EGR2) gene are associated with hereditary myelinopathies. Nat Genet 18:382–384.

Weiss HD, Walker MD, Wiernik PH (1974). Neurotoxicity of commonly used antineoplastic agents (second of two parts). N Engl J Med 291:127–133.

Yoshihara T, Kanda F, Yamamoto M, Ishihara H, Misu K, Hattori N, Chihara K, Sobue G (2001). A novel missense mutation in the early growth response 2 gene are associated with late-onset Charcot-Marie-Tooth disease type 1. J Neurol Sci 184:149–153.

Journal of Medical Virology 84:1120–1127 (2012)

Human T-Lymphotropic Virus Type I (HTLV-I)-Specific CD8+ Cells Accumulate in the Lungs of Patients Infected With HTLV-I With Pulmonary Involvement

Takashi Kawabata,[1] Ikkou Higashimoto,[1] Hiroshi Takashima,[2] Shuji Izumo,[3] and Ryuji Kubota[3]*

[1]*Department of Respiratory Medicine, Graduate School of Medical and Dental Sciences, Kagoshima University, Kagoshima, Japan*
[2]*Department of Neurology and Geriatrics, Graduate School of Medical and Dental Sciences, Kagoshima University, Kagoshima, Japan*
[3]*Center for Chronic Viral Diseases, Graduate School of Medical and Dental Sciences, Kagoshima University, Kagoshima, Japan*

Pulmonary involvement has been identified in human T-lymphotropic virus type I (HTLV-I) carriers and patients with HTLV-I-associated myelopathy/tropical spastic paraparesis (HAM/TSP). However, the relationship between HTLV-I infection and lung disease is poorly understood. The occurrence of HTLV-I-specific immune responses in the lungs of patients infected with HTLV-I with pulmonary involvement was investigated. The frequency of HTLV-I-specific CD8+ cells and the amount of HTLV-I proviral DNA were determined in bronchoalveolar lavage fluid cells and peripheral blood mononuclear cells (PBMCs) from five patients with HAM/TSP and one HTLV-I carrier who had pulmonary involvement. HTLV-I-specific CD8+ cells were detected by flow cytometry using human leukocyte antigen/antigen complex multimers. The analysis of bronchoalveolar lavage fluid revealed lymphocytosis in five of six patients. HTLV-I provirus was detected in the bronchoalveolar lavage fluid cells of all patients, and the proviral load in these cells was comparable to that in PBMCs. The frequency of HTLV-I-specific CD8+ cells in the bronchoalveolar lavage fluid cells was 5.1 times higher than that in PBMCs. Immunohistochemically, clusters formed by HTLV-I-specific CD8+ cells were detected in lung tissue by in situ tetramer staining. No samples were available from patients infected with HTLV-I without lung disorders. Whether accumulation of CD8+ cells is specific to patients with pulmonary involvement remains unclear. These results indicate that HTLV-I-specific CD8+ cells accumulate and HTLV-I-infected cells exist in the lungs of patients infected with HTLV-I with pulmonary involvement. ***J. Med. Virol. 84:1120–1127, 2012.*** © 2012 Wiley Periodicals, Inc.

KEY WORDS: HTLV-I; lung; bronchoalveolar lavage fluid; CD8+ cells; proviral load

INTRODUCTION

Human T-lymphotropic virus type I (HTLV-I), a human retrovirus, is the etiological agent of adult T-cell leukemia, a hematological malignancy of CD4+ T lymphocytes [Uchiyama et al., 1977]. HTLV-I is also responsible for several inflammatory disorders, including HTLV-I-associated myelopathy/tropical spastic paraparesis (HAM/TSP), HTLV-I-associated uveitis and HTLV-I-associated arthropathy [Gessain et al., 1985; Osame et al., 1986; Nishioka et al., 1989; Mochizuki et al., 1992]. Pulmonary involvement has also been reported in patients infected with HTLV-I [Kimura et al., 1986; Maruyama et al., 1988]. A radiological study revealed that the incidence of

Grant sponsor: Japanese Ministry of Education, Culture, Sports, Science and Technology.

Conflicts of interest: None.

*Correspondence to: Ryuji Kubota, MD, Center for Chronic Viral Diseases, Graduate School of Medical and Dental Sciences, Kagoshima University, 8-35-1 Sakuragaoka, Kagoshima 890-8544, Japan. E-mail: kubotar@m2.kufm.kagoshima-u.ac.jp

Accepted 20 March 2012

DOI 10.1002/jmv.23307
Published online in Wiley Online Library (wileyonlinelibrary.com).

pulmonary involvement is higher in HTLV-I carriers than in non-infected individuals [Okada et al., 2006]. In HTLV-I carriers, HTLV-I infection increases the risk for pulmonary cryptococcosis, tuberculosis, and community-acquired pneumonia [Kohno et al., 1992; Marinho et al., 2005; Atsumi et al., 2009]. In patients with adult T-cell leukemia, pulmonary involvement is mainly caused by opportunistic infections or pulmonary infiltration of leukemic cells [Yoshioka et al., 1985]. Other pulmonary involvement has been observed in HTLV-I carriers and patients with HAM/TSP. Importantly, analysis of bronchoalveolar lavage fluid obtained from these patients revealed marked lymphocytosis [Sugimoto et al., 1987]. These findings may indicate that HTLV-I infection can contribute to inflammatory lung diseases.

HTLV-I-associated lung disease has various pulmonary manifestations, including bronchiolitis, alveolitis, diffuse panbronchiolitis, and interstitial pneumonia [Setoguchi et al., 1991; Kikuchi et al., 1996; Sugimoto et al., 1998]. Several studies have identified pulmonary involvement specific to HTLV-I-associated lung disease. HTLV-I proviral load in peripheral blood mononuclear cells (PBMCs) correlates with the degree of bronchoalveolar lymphocytosis [Mori et al., 2005], and mRNA of the HTLV-I gene is upregulated in bronchoalveolar lavage fluid cells than in PBMCs [Higashiyama et al., 1994; Seki et al., 2000b]. Patients with HTLV-I-associated lung disease have elevated levels of soluble adhesion molecules and soluble interleukin-2 receptor α in bronchoalveolar lavage fluid and increased mRNA levels of cytokines and chemokines in bronchoalveolar lavage fluid cells [Sugimoto et al., 1989; Seki et al., 1999; Yamazato et al., 2003]. These data suggest that HTLV-I infection induces pulmonary inflammation. However, the immunological parameters measured in the above studies are not specific for HTLV-I, and whether HTLV-I-induced inflammation may occur in the lungs remains unclear. The objective of this study was to investigate whether HTLV-I-specific immune responses occur in the lungs of patients infected with HTLV-I with pulmonary involvement using peptide/human leukocyte antigen (HLA) complex multimers.

MATERIALS AND METHODS

Subjects

The study subjects evaluated at Kagoshima University Hospital from 1994 to 2008 included five patients with HAM/TSP and one HTLV-I carrier who had pulmonary involvement (Table I). The selection criteria for inclusion in the study were as follows: (1) both PBMCs and bronchoalveolar lavage fluid cells had to be obtained and (2) the patients had to have specific HLAs (HLA-A*0201 or -A*2402) because HTLV-I Tax11–19 and Tax301–309 epitopes are well characterized and represent strong immunodominant epitopes restricted to these HLAs [Yashiki et al., 2001; Kozako et al., 2006]. HLA was determined by polymerase chain reaction (PCR) with sequence-specific primers as described previously [Bunce et al., 1995]. The serum titre of anti-HTLV-I antibody was measured by the particle agglutination method (Serodia-HTLV-I; Fujirebio, Tokyo, Japan), and HAM/TSP was diagnosed according to WHO criteria. HTLV-I status and clinical condition of the lungs are shown in Tables I and II, respectively. After obtaining informed consent, fiberoptic bronchoscopy and bronchoalveolar lavage were performed in these patients. Bronchoalveolar lavage fluid cells and PBMCs were obtained under written informed consent and stored in liquid nitrogen until use. This study was reviewed and approved by the Kagoshima University Ethical Committee and was conducted in accordance with the Declaration of Helsinki.

Quantitative PCR for HTLV-I Provirus

Genomic DNA was extracted from PBMCs and bronchoalveolar lavage fluid cells using a commercial kit (Qiagen, Tokyo, Japan). A quantitative PCR assay was performed as described previously [Nagai et al., 1998].

Flow Cytometry

HLA-A*0201/HTLV-I Tax11–19 and HLA-A*2402/HTLV-I Tax301–309 pentamers labeled with phycoerythrin (PE) were purchased from Proimmune (Oxford,

TABLE I. Clinical Characteristics of the Patients

No.	Age	Sex	HTLV-I status	Duration (years)[a]	HTLV-I Ab[b]	HLA[c]
1	63	F[d]	HAM[e]/SjS[f]	7	×65536	A*24
2	81	F	carrier	N/A[g]	×32768	A*24
3	55	F	HAM	3	×4096	A*02
4	65	F	HAM	7	×4096	A*24
5	54	F	HAM/SjS	2	×65536	A*24
6	36	F	HAM	3	×64	A*24

[a]Duration of HAM/TSP in years.
[b]Serum antibody titre as determined by the agglutination method.
[c]Human leukocyte antigen.
[d]Female.
[e]HAM/TSP.
[f]Sjögren syndrome.
[g]Not applicable.

TABLE II. Clinical Condition of Patient Lungs

No.	Chest computed tomography findings	Smoking	Bacterial feature
1	Partial bronchiectasis and centrilobular nodules	N[a]	Not examined
2	Lobular centrilobular nodules and bronchiectasis	N	*M. intracellulare*
3	Lobular centrilobular nodules and bronchiectasis	N	*Micrococcus sp*
4	Diffuse centrilobular nodules and bronchiectasis	C[b]	*H. influenzae*
5	A few centrilobular nodules	N	*Staphylococcus*
6	Hyperinflation	N	*H. parainfluenzae*

[a]Never smokers.
[b]Current smokers.

UK) [Ogg and McMichael, 1998]. Bronchoalveolar lavage fluid cells or PBMCs were stained with HTLV-I Tax pentamer or HIV Gag pentamer (control) followed by PE–Cy5-conjugated anti-CD8 antibody (clone T8; Beckman Coulter, Tokyo, Japan). The cells were analysed using an Epics XL flow cytometer (Beckman Coulter, Tokyo, Japan) with Expo32 software. Lymphocytes, determined on the basis of forward and side scatter, were gated for CD8 high cells, and the frequency of HTLV-I-specific CD8+ cells stained with the pentamers was determined in this gate.

Immunohistological Analysis

A biopsy of the lower lung was obtained by video-assisted thoracoscopic surgery from a 65-year-old woman with HTLV-I infection. She also had HAM/TSP, bronchiolitis obliterans, and HLA-A*2402. In situ detection of antigen-specific T cells using tetramers was performed according to previously published methods with some modifications [Skinner et al., 2000]. In brief, an 8-μm-thick tissue section was incubated with HLA-A*2402/HTLV-I Tax301–309 tetramer labeled with PE (MBL, Nagoya, Japan) and mouse anti-CD8 antibody (clone DK25, mouse IgG1; Dako, Tokyo, Japan) at 4°C overnight. After fixation with 4% paraformaldehyde, the section was incubated with rabbit anti-PE antibody (BioGenesis, Poole, UK) followed by a combination of Alexa Fluor 488-conjugated goat anti-rabbit antibody (Invitrogen, Tokyo, Japan) and Alexa Fluor 594-conjugated goat anti-mouse IgG1 antibody. The section was finally stained with 4′, 6-diamidino-2-phenylindole. The fluorescence signal was detected using a confocal laser scanning microscope (FV500; Olympus, Tokyo, Japan). For in situ detection of HTLV-I-infected cells, a section was fixed with 4% paraformaldehyde and incubated with a combination of anti-HTLV-I Tax antibody (Lt-4, mouse IgG3) [Lee et al., 1989] and anti-CD4 antibody (4B12, mouse IgG1; Dako) or with a combination of anti-HTLV-I Gag antibody (TP-7, mouse IgG1; Abcam, Cambridge, UK) and rat anti-CD4 antibody (YNB46.1.8; Abcam), followed by appropriate secondary antibodies labeled with fluorochrome.

Statistical Analysis

Wilcoxon signed-rank test and Spearman's rank correlation test were used for statistical analysis with StatView version J5.0. A P-value of <0.05 was considered to be significant.

RESULTS

Lymphocytosis in Bronchoalveolar Lavage Fluid From Patients Infected With HTLV-I

The cell count in bronchoalveolar lavage fluid was increased in the HTLV-I carrier (patient 2) and two of five patients with HAM/TSP (patients 5 and 6; Table III). Patient 4 was a smoker whose cell count

TABLE III. Cellular Composition of Bronchoalveolar Lavage Fluid in the Patients

No.	Cell count ($\times 10^5$/ml)	Macrophages (%)	Lymphocytes (%)	Neutrophils (%)	Eosinophils (%)
1	0.68	49.0	47.7	0.7	1.0
2	1.76	52.3	22.0	24.7	0.7
3	0.57	91.6	6.2	2.0	0.2
4	1.52	67.6	19.2	13.1	0.1
5	1.87	40.0	50.0	3.0	0.2
6	1.23	62.0	37.2	0.8	0.0
NS[a]	0.61 ± 0.36[b]	88.0 ± 9.9	11.0 ± 9.3	0.7 ± 1.6	0.3 ± 0.6
CS[c]	2.38 ± 1.58	95.7 ± 3.8	3.6 ± 3.1	0.5 ± 1.6	0.2 ± 0.5

[a]Never smokers.
[b]Mean ± SD. Values are from data published by the BAL Cooperative Group Steering Committee [Anonymous, 1990].
[c]Current smokers.

TABLE IV. HTLV-I Proviral Loads and HTLV-I Tax-Specific CD8+ Cells in PBMCs and Bronchoalveolar Fluid Cells

	PBMCs					
No.	CD4+ (%)	CD8+ (%)	CD4/8	PVL[a]	PVL/CD4[b]	Pentamer+/CD8[c] (%)
1	30.64	13.71	2.23	16.37	82.89	0.90
2	29.52	57.30	0.52	3.92	16.80	2.78
3	32.66	29.56	1.10	3.91	15.29	0.15
4	19.53	14.99	1.30	7.25	86.72	0.96
5	54.83	17.19	3.18	4.94	11.02	3.54
6	41.43	32.34	1.28	39.60	129.38	0.64
Mean	34.77	27.52	1.60	12.70	57.02	1.50
SD	12.07	16.55	0.95	14.00	19.52	1.34

	Bronchoalveolar fluid cells[d]					
CD4+ (%)	CD4+ (%)	CD4/8	PVL	PVL/CD4	Pentamer+/CD8 (%)	Pentamer+ ratio[d]
69.02	10.65	6.48	22.75	66.34	2.90	3.22
72.09	9.27	7.86	2.40	8.58	18.99	6.83
24.24	14.99	1.61	3.53	37.91	0.16	1.07
23.26	63.74	0.36	3.57	33.47	2.52	2.63
68.71	25.00	2.75	29.18	68.76	19.56	5.52
37.85	39.50	0.96	27.92	93.24	1.61	2.52
49.20	27.19	3.34	14.90	51.38	7.62	3.63
23.33	21.15	3.10	13.00	30.37	9.08	2.13

[a]HTLV-I proviral loads (PVL) in total cells (copy/10^2 cells).
[b]HTLV-I PVL in CD4+ cells (copy/10^2 CD4+ cells).
[c]Percentage of pentamer+ HTLV-I Tax-specific CD8+ cells in CD8+ cells.
[d]Ratio of percentage of pentamer+ HTLV-I Tax-specific CD8+ cells in bronchoalveolar fluid cells to that in PBMCs.

was within the normal range. Lymphocytosis was observed in five of six patients except in patient 3 (Table III). Percentages of CD4+ and CD8+ cells were analysed by flow cytometry, and CD4/8 ratios in PBMCs and bronchoalveolar lavage fluid cells were 1.60 and 3.34, respectively (Table IV).

HTLV-I Proviral Loads in Bronchoalveolar Lavage Fluid Cells and PBMCs

The HTLV-I proviral load in PBMCs and bronchoalveolar lavage fluid cells of the patients was determined by quantitative PCR. HTLV-I was detected in all tested samples (Table IV). No difference was observed in the HTLV-I proviral load in the DNA extracted from PBMCs and bronchoalveolar lavage fluid cells (12.70 and 14.90 copies/10^2 cells, respectively; $P = 0.92$). The cellular composition differs between PBMCs and bronchoalveolar lavage fluid cells, and HTLV-I predominantly infects CD4+ cells in vivo [Richardson et al., 1990]. Therefore, the HTLV-I proviral load was calculated in 10^2 CD4+ cells from PBMCs and bronchoalveolar lavage fluid cells according to the following formula: (proviral load in 10^2 total cells)/[(percentage of lymphocytes in total cells) × (percentage of CD4+ cells in lymphocytes)] × 10^4. No significant difference was observed in the proviral load in 10^2 CD4+ cells from PBMCs and bronchoalveolar lavage fluid cells (57.02 and 51.38 copies, respectively; $P = 0.75$; Table IV).

Increased HTLV-I-Specific CD8+ Cells in Bronchoalveolar Lavage Fluid Cells Than in PBMCs

Whether HTLV-I-specific CD8+ cells were increased in the lungs of patients infected with HTLV-I was investigated using HTLV-I Tax epitope/HLA pentamers. Figure 1 shows the results of a representative flow cytometric analysis in which the frequency of HTLV-I Tax-specific CD8+ cells was determined in CD8 high lymphocytes. The frequency of the CD8+ cells in bronchoalveolar lavage fluid cells was increased compared with that in PBMCs (Fig. 2A, $P = 0.028$). The mean frequency of HTLV-I-specific CD8+ cells was 1.50% in PBMCs and 7.62% in bronchoalveolar lavage fluid cells (Table IV). The frequency in bronchoalveolar lavage fluid cells was 5.1 times higher than that in PBMCs. In addition, the frequency of HTLV-I Tax-specific CD8+ cells in bronchoalveolar lavage fluid cells correlated well with that in PBMCs (Fig. 2B, $P = 0.035$).

Correlation of HTLV-I Proviral Loads With HTLV-I-Specific CD8+ Cells

Whether the HTLV-I proviral load correlated with HTLV-I-specific CD8+ cell responses was investigated. The frequency of HTLV-I-specific CD8+ cells tended to correlate negatively with the proviral load in both PBMCs and bronchoalveolar lavage fluid cells, although this was not statistically significant (Fig. 3).

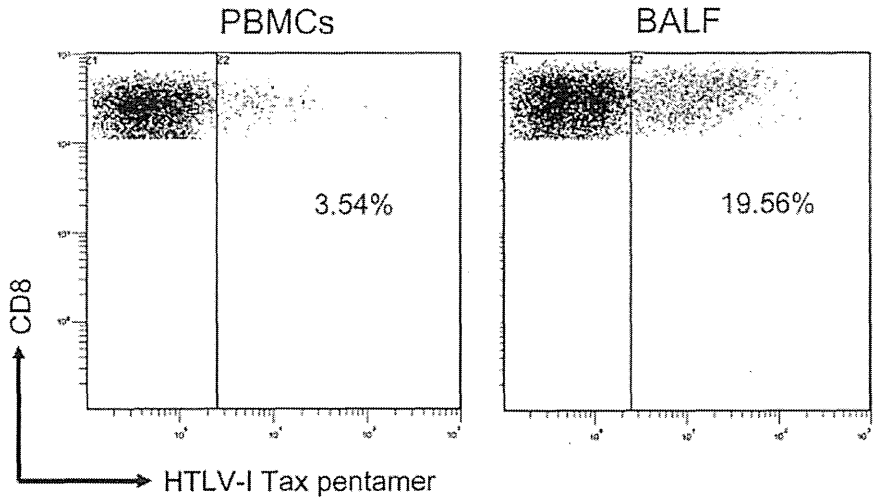

Fig. 1. Representative flow cytometric detection of HTLV-I Tax-specific CD8+ cells in PBMCs and bronchoalveolar lavage fluid cells. PBMCs and bronchoalveolar lavage fluid cells (BALF) were obtained from six subjects with HTLV-I infection. Lymphocytes were gated on the basis of forward and side scatter, and the CD8 high population was gated. The frequency of HTLV-I Tax pentamer-positive cells was determined in the CD8+ cells in PBMCs and bronchoalveolar lavage fluid cells. The figures are representative data from patient 5, and the numbers indicate the pentamer-positive cells as a percentage of total CD8 high cells.

In situ Tetramer Staining of HTLV-I Tax-Specific CD8+ Cells

In situ detection of CD8+ cells using HTLV-I Tax tetramer was performed using lung tissue from a patient with HAM/TSP and bronchiolitis obliterans. CD4+ and CD8+ cells were distributed in the alveolar septa. As shown in Figure 4, HLA-A*2402/HTLV-I Tax301–309-specific CD8+ cells detected in lung tissue formed clusters. Tetramer staining was co-localized with CD8 molecules in the positive cells from the tissue (Fig. 4A). In contrast, no cells in lung tissue from the same patient were stained with the negative control HLA-A*2402/HIV Gag tetramer (Fig. 4B). In addition, no cells were stained with HLA-A*2402/HTLV-I Tax301–309 tetramer in lung tissue from a patient who was HLA-A*2402 positive but HTLV-I negative (Fig. 4C). Whether HTLV-I proteins could be detected in lung tissue was examined using anti-HTLV-I Tax and Gag antibodies. However, no HTLV-I proteins were found (data not shown).

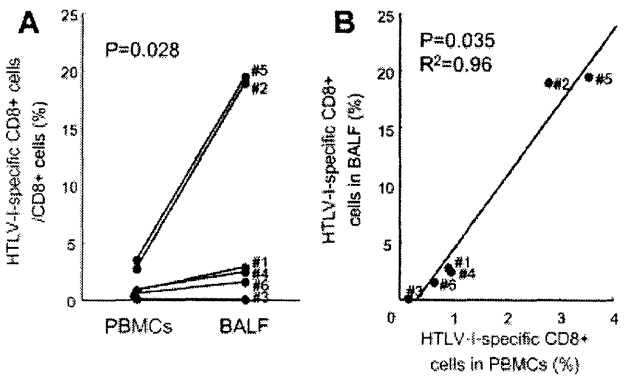

Fig. 2. Frequency of HTLV-I Tax-specific CD8+ cells in PBMCs and bronchoalveolar lavage fluid cells. **A**: The frequency of HTLV-I Tax-specific CD8+ cells was significantly increased in bronchoalveolar lavage fluid cells (BALF) than in PBMCs according to Wilcoxon signed-rank test. **B**: The frequency of HTLV-I Tax-specific CD8+ cells in bronchoalveolar lavage fluid cells significantly correlated with that in PBMCs according to Spearman's rank correlation test.

DISCUSSION

In this study, HTLV-I-specific CD8+ cells were present at a markedly higher frequency in bronchoalveolar lavage fluid cells than in PBMCs of all patients studied (Fig. 2A and Table IV). In terms of bacterial species cultured from sputum samples, patient 2 was positive for *Mycobacterium intracellulare*, patient 4 was positive for *Haemophilus influenzae*, and the other patients were positive for normal oral flora (Table II). HTLV-I-specific CD8+ cells were found to be circulating in the body of a patient infected with HTLV-I. A small minority of the CD8+ cells may infiltrate non-specifically inflamed tissues, even if inflammation was caused by microorganisms other than HTLV-I. However, in this study, HTLV-I-specific CD8+ cells accumulated at a 5.1 times higher frequency in bronchoalveolar lavage fluid cells than in PBMCs (Table IV), which suggests that the CD8+ cells selectively infiltrated the lungs and that HTLV-I-specific immune responses occurred in the lungs of these patients. In situ tetramer staining

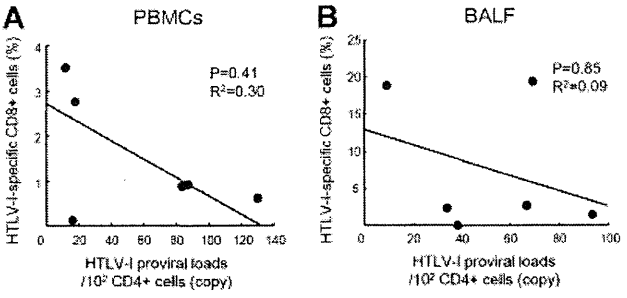

Fig. 3. The relationship between HTLV-I proviral load and frequency of HTLV-I Tax-specific CD8+ cells in PBMCs and bronchoalveolar lavage fluid cells. The frequency of HTLV-I Tax-specific CD8+ cells in CD8+ cells was plotted against HTLV-I proviral loads in CD4+ cells in PBMCs (**A**) and in bronchoalveolar lavage fluid cells (BALF) (**B**). Negative correlations were observed in both PBMCs and bronchoalveolar lavage fluid cells, but these were not statistically significant according to Spearman's rank correlation test.

revealed that HTLV-I-specific CD8+ cells formed clusters in the lung tissue, further supporting the above proposition (Fig. 4). In addition, the frequency of HTLV-I-specific CD8+ cells in the bronchoalveolar lavage fluid cells correlated with that in PBMCs (Fig. 2B), which suggests that the increased frequency of HTLV-I-specific CD8+ cells in peripheral blood drives an efficient infiltration of these CD8+ cells into the lungs.

No bronchoalveolar lavage fluid was obtained from patients infected with HTLV-I without pulmonary involvement. Therefore, whether accumulation of HTLV-I-specific CD8+ cells in the lungs is associated with pulmonary involvement or a common phenomenon in patients infected with HTLV-I remains unclear. Further studies are needed to elucidate this point. Cells stained with antigen/HLA class I complex multimers contain not only effector/memory cells but also naïve cells; therefore, some multimer-positive

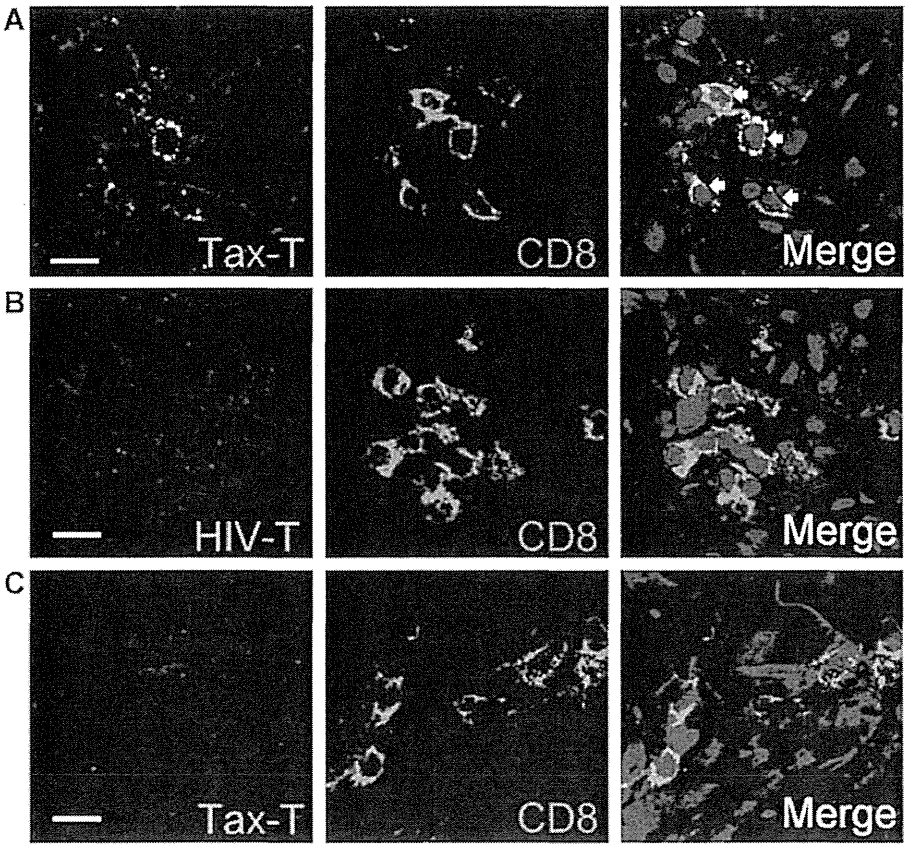

Fig. 4. In situ detection of HTLV-I Tax-specific CD8+ cells in a patient with HAM/TSP and bronchiolitis obliterans. A video-assisted thoracoscopic biopsy was performed in a 65-year-old woman with HAM/TSP and bronchiolitis obliterans who was HLA-A*2402 positive. Sections from the frozen lung tissue were stained with tetramers (Tax-T; green) and anti-CD8 antibody (red). **A**: Staining with HLA-A*2402/HTLV-I Tax301–309 tetramer overlapped with CD8 staining, yielding a yellow color in the merged image (left, arrowed). Tetramer-positive cells were observed in the alveolar septa localized within a cluster. **B**: No cells were stained with HLA-A*2402/HIV Gag tetramer (HIV-T) in the serial section from the same patient. **C**: No cells were stained with HLA-A*2402/HTLV-I Tax301–309 tetramer (Tax-T) in the control sample from a patient positive for HLA-A*2402 but negative for HTLV-I infection. Original magnification is ×400. The bars indicate 10 μm.

cells are inert cytotoxic T lymphocytes [Goulder et al., 2000]. It would be important to know how many HTLV-I-specific CD8+ cells are functional cytotoxic T lymphocytes against HTLV-I and whether the cytotoxic activity of the cells differs between bronchoalveolar lavage fluid cells and PBMCs. However, because the sample number was limited, this could not be determined in this study. Further analysis including cytotoxic activity is needed to understand the role of accumulation of the CD8+ cells in the lungs.

A range of pulmonary involvement in patients infected with HTLV-I has recently been described in a study using computed tomography to analyse samples from 320 HTLV-I carriers [Okada et al., 2006]. The pulmonary manifestations included centrilobular nodules, thickening of bronchovascular bundles, ground–glass opacity, bronchiectasis, interlobular septal thickening, and consolidation. Pathologically, these findings correspond to lymphocytic infiltration along respiratory bronchioles and bronchovascular bundles. In the present study, all patients showed changes in the peripheral bronchioles in computed tomography images. Peripheral bronchioles and alveoli have been emphasized as an important lesion site in HTLV-I-associated lung disease, probably because the marked lymphocytosis in bronchoalveolar lavage fluid is a characteristic of the disease [Sugisaki et al., 1998]. However, the respiratory tract may be another affected lesion in HTLV-I-associated lung disease.

HTLV-I-infected cells are activated and express various chemokine receptors and increased adhesion molecules on the surface in peripheral blood, suggesting that the cells have an enhanced ability to migrate into tissue sites [Seki et al., 1999; Yamazato et al., 2003]. Previous studies reported that lymphocytosis in bronchoalveolar lavage fluid is observed not only in HTLV-I-infected patients with abnormal lung images but also in infected individuals with apparently normal lungs [Seki et al., 2000a]. In the present study, the patients who had less abnormal lung images showed an accumulation of HTLV-I-specific CD8+ cells in the lungs (patients 1, 5, and 6 in Table IV). Taken together, these results suggest that inflammation can be induced in the lung by HTLV-I infection even in the absence of apparent clinical manifestations [Sugisaki et al., 1998].

In summary, HTLV-I-specific CD8+ cells accumulate and HTLV-I-infected cells exist in the lungs of patients infected with HTLV-I with pulmonary involvement. These results suggest that an interaction between HTLV-I-infected cells and HTLV-I-specific CD8+ cells may occur in the lung of patients infected with HTLV-I. Further studies to clarify clinical features of the lung specifically associated with HTLV-I infection are needed.

ACKNOWLEDGMENTS

We thank Ms. Takako Inoue and Noriko Hirata for their excellent technical assistance.

REFERENCES

Anonymous. 1990. Bronchoalveolar lavage constituents in healthy individuals, idiopathic pulmonary fibrosis, and selected comparison groups. Am Rev Respir Dis 141:s169.

Atsumi E, Yara S, Higa F, Hirata T, Haranaga S, Tateyama M, Fujita J. 2009. Influence of human T lymphotropic virus type I infection on the etiology of community-acquired pneumonia. Intern Med 48:959–965.

Bunce M, O'Neill CM, Barnardo MC, Krausa P, Browning MJ, Morris PJ, Welsh KI. 1995. Phototyping: Comprehensive DNA typing for HLA-A, B, C, DRB1, DRB3, DRB4, DRB5 & DQB1 by PCR with 144 primer mixes utilizing sequence-specific primers (PCR-SSP). Tissue Antigens 46:355–367.

Gessain A, Barin F, Vernant JC, Gout O, Maurs L, Calender A, de The G. 1985. Antibodies to human T-lymphotropic virus type-I in patients with tropical spastic paraparesis. Lancet 2:407–410.

Goulder PJ, Tang Y, Brander C, Betts MR, Altfeld M, Annamalai K, Trocha A, He S, Rosenberg ES, Ogg G, O'Callaghan CA, Kalams SA, McKinney RE Jr, Mayer K, Koup RA, Pelton SI, Burchett SK, McIntosh K, Walker BD. 2000. Functionally inert HIV-specific cytotoxic T lymphocytes do not play a major role in chronically infected adults and children. J Exp Med 192:1819–1832.

Higashiyama Y, Katamine S, Kohno S, Mukae H, Hino S, Miyamoto T, Hara K. 1994. Expression of human T lymphotropic virus type 1 (HTLV–1) tax/rex gene in fresh bronchoalveolar lavage cells of HTLV-1-infected individuals. Clin Exp Immunol 96:193–201.

Kikuchi T, Saijo Y, Sakai T, Abe T, Ohnuma K, Tezuka F, Terunuma H, Ogata K, Nukiwa T. 1996. Human T-cell lymphotropic virus type I (HTLV-I) carrier with clinical manifestations characteristic of diffuse panbronchiolitis. Intern Med 35:305–309.

Kimura I, Tsubota T, Tada S, Sogawa J. 1986. Presence of antibodies against adult T cell leukemia antigen in the patients with chronic respiratory diseases. Acta Med Okayama 40:281–284.

Kohno S, Koga H, Kaku M, Yasuoka A, Maesaki S, Tanaka K, Mitsutake K, Matsuda H, Araki J, Hara K. 1992. Prevalence of HTLV-I antibody in pulmonary cryptococcosis. Tohoku J Exp Med 167:13–18.

Kozako T, Arima N, Toji S, Masamoto I, Akimoto M, Hamada H, Che XF, Fujiwara H, Matsushita K, Tokunaga M, Haraguchi K, Uozumi K, Suzuki S, Takezaki T, Sonoda S. 2006. Reduced frequency, diversity, and function of human T cell leukemia virus type 1-specific CD8+ T cell in adult T cell leukemia patients. J Immunol 177:5718–5726.

Lee B, Tanaka Y, Tozawa H. 1989. Monoclonal antibody defining tax protein of human T-cell leukemia virus type-I. Tohoku J Exp Med 157:1–11.

Marinho J, Galvao-Castro B, Rodrigues LC, Barreto ML. 2005. Increased risk of tuberculosis with human T-lymphotropic virus-1 infection: A case-control study. J Acquir Immune Defic Syndr 40:625–628.

Maruyama I, Chihara J, Sakashita I, Mizoguchi R, Mori S, Usuku K, Jonosono M, Tara M, Matsumoto S, Niina S, Sonoda S, Yashiki S, Osame M. 1988. HTLV-I associated bronchopneumonopathy, a new clinical entity? Am Rev Respir Dis 137:46.

Mochizuki M, Watanabe T, Yamaguchi K, Yoshimura K, Nakashima S, Shirao M, Araki S, Takatsuki K, Mori S, Miyata N. 1992. Uveitis associated with human T-cell lymphotropic virus type I. Am J Ophthalmol 114:123–129.

Mori S, Mizoguchi A, Kawabata M, Fukunaga H, Usuku K, Maruyama I, Osame M. 2005. Bronchoalveolar lymphocytosis correlates with human T lymphotropic virus type I (HTLV-I) proviral DNA load in HTLV-I carriers. Thorax 60:138–143.

Nagai M, Usuku K, Matsumoto W, Kodama D, Takenouchi N, Moritoyo T, Hashiguchi S, Ichinose M, Bangham CR, Izumo S, Osame M. 1998. Analysis of HTLV-I proviral load in 202 HAM/TSP patients and 243 asymptomatic HTLV-I carriers: High proviral load strongly predisposes to HAM/TSP. J Neurovirol 4:586–593.

Nishioka K, Maruyama I, Sato K, Kitajima I, Nakajima Y, Osame M. 1989. Chronic inflammatory arthropathy associated with HTLV-I. Lancet 1:441.

Ogg GS, McMichael AJ. 1998. HLA-peptide tetrameric complexes. Curr Opin Immunol 10:393–396.

Okada F, Ando Y, Yoshitake S, Yotsumoto S, Matsumoto S, Wakisaka M, Maeda T, Mori H. 2006. Pulmonary CT findings in 320 carriers of human T-lymphotropic virus type 1. Radiology 240:559–564.

Osame M, Usuku K, Izumo S, Ijichi N, Amitani H, Igata A, Matsumoto M, Tara M. 1986. HTLV-I associated myelopathy, a new clinical entity. Lancet 1:1031–1032.

Richardson JH, Edwards AJ, Cruickshank JK, Rudge P, Dalgleish AG. 1990. In vivo cellular tropism of human T-cell leukemia virus type 1. J Virol 64:5682–5687.

Seki M, Higashiyama Y, Kadota J, Mukae H, Yanagihara K, Tomono K, Kohno S. 2000a. Elevated levels of soluble adhesion molecules in sera and BAL fluid of individuals infected with human T-cell lymphotropic virus type 1. Chest 118:1754–1761.

Seki M, Higashiyama Y, Mizokami A, Kadota J, Moriuchi R, Kohno S, Suzuki Y, Takahashi K, Gojobori T, Katamine S. 2000b. Up-regulation of human T lymphotropic virus type 1 (HTLV-1) tax/rex mRNA in infected lung tissues. Clin Exp Immunol 120:488–498.

Seki M, Kadota JI, Higashiyama Y, Iida K, Iwashita T, Sasaki E, Maesaki S, Tomono K, Kohno S. 1999. Elevated levels of beta-chemokines in bronchoalveolar lavage fluid (BALF) of individuals infected with human T lymphotropic virus type-1 (HTLV-1). Clin Exp Immunol 118:417–422.

Setoguchi Y, Takahashi S, Nukiwa T, Kira S. 1991. Detection of human T-cell lymphotropic virus type I-related antibodies in patients with lymphocytic interstitial pneumonia. Am Rev Respir Dis 144:1361–1365.

Skinner PJ, Daniels MA, Schmidt CS, Jameson SC, Haase AT. 2000. Cutting edge: In situ tetramer staining of antigen-specific T cells in tissues. J Immunol 165:613–617.

Sugimoto M, Kitaichi M, Ikeda A, Nagai S, Izumi T. 1998. Chronic bronchioloalveolitis associated with human T-cell lymphotrophic virus type I infection. Curr Opin Pulm Med 4:98–102.

Sugimoto M, Nakashima H, Matsumoto M, Uyama E, Ando M, Araki S. 1989. Pulmonary involvement in patients with HTLV-I-associated myelopathy: Increased soluble IL-2 receptors in bronchoalveolar lavage fluid. Am Rev Respir Dis 139:1329–1335.

Sugimoto M, Nakashima H, Watanabe S, Uyama E, Tanaka F, Ando M, Araki S, Kawasaki S. 1987. T-lymphocyte alveolitis in HTLV-I-associated myelopathy. Lancet 2:1220.

Sugisaki K, Tsuda T, Kumamoto T, Akizuki S. 1998. Clinicopathologic characteristics of the lungs of patients with human T cell lymphotropic virus type 1-associated myelopathy. Am J Trop Med Hyg 58:721–7725.

Uchiyama T, Yodoi J, Sagawa K, Takatsuki K, Uchino H. 1977. Adult T-cell leukemia: Clinical and hematologic features of 16 cases. Blood 50:481–492.

Yamazato Y, Miyazato A, Kawakami K, Yara S, Kaneshima H, Saito A. 2003. High expression of p40(tax) and pro-inflammatory cytokines and chemokines in the lungs of human T-lymphotropic virus type 1-related bronchopulmonary disorders. Chest 124: 2283–2292.

Yashiki S, Fujiyoshi T, Arima N, Osame M, Yoshinaga M, Nagata Y, Tara M, Nomura K, Utsunomiya A, Hanada S, Tajima K, Sonoda S. 2001. HLA-A*26, HLA-B*4002, HLA-B*4006, and HLA-B*4801 alleles predispose to adult T cell leukemia: The limited recognition of HTLV type 1 tax peptide anchor motifs and epitopes to generate anti-HTLV type 1 tax CD8(+) cytotoxic T lymphocytes. AIDS Res Hum Retroviruses 17:1047–1061.

Yoshioka R, Yamaguchi K, Yoshinaga T, Takatsuki K. 1985. Pulmonary complications in patients with adult T-cell leukemia. Cancer 55:2491–2494.

LETTER

Inflammatory radiculoneuropathy in an ALS4 patient with a novel *SETX* mutation

INTRODUCTION

Amyotrophic lateral sclerosis 4 (ALS4), a rare form of autosomal dominant juvenile-onset ALS characterised by slow progression and sparing of bulbar and respiratory muscles,[1 2] results from missense mutations in the *senataxin* (*SETX*) gene.[3] This study reports the clinical pathology of a male Japanese ALS4 patient carrying a novel mutation in the *SETX* gene who presented with coexistent inflammatory radiculoneuropathy.

CASE REPORT

Slight delays in early development resulted in the patient beginning to walk at 1.5 years. He was prone to falls and had suffered from pes cavus since childhood. At 35 years of age, the patient presented with difficulty walking. One year later he found it difficult to fully extend his fingers and this was exacerbated over the following 3 months. Nerve conduction studies revealed asymmetric demyelinating patterns (median nerve motor conduction velocity: right 29 m/s, left 53 m/s). Subsequently, the patient developed a neurogenic bladder. Intravenous immunoglobulin therapy (20 g/day for 5 days) resulted in mild improvement in muscle weakness (one point on the manual muscle test) and in the amplitude of compound motor action potentials for the median (right 1.982 mV to 3.362 mV, left 1.342 mV to 2.062 mV) and right ulnar nerve (6.064 mV to 8.296 mV). At 37 years of age, the patient developed progressive distal weakness and sensory disturbances in the right forearm and medial thigh. Following two courses of intravenous methylprednisolone (1 g/day for 3 days; steroid pulse therapy) and subsequent oral prednisolone treatment (50 mg/day with gradual tapering), sensory impairment and muscle weakness both improved. Thereafter, the patient underwent repeated steroid pulse therapy when muscle weakness became worse. At 41 years of age, the patient again experienced exaggerated distal weakness and dysuria and was admitted to our department. The patient had no family history of similar degenerative diseases.

Long, thin limbs, right hand drop, bilateral pes cavus, and distal-dominant amyotrophy and limb weakness were observed (figure 1A–D). However, the patient exhibited no respiratory or bulbar weakness. Fasciculation was visible in the trunk and limbs. Brisk tendon reflexes of the limbs and ankle clonus were present. Hypoesthesia and hyperalgesia were present in the right arm and bilaterally below the Th9 level. The patient suffered from shoulder pain and increased vibratory thresholds in the feet. In addition, he experienced dysuria, which required intermittent self-catheterisation.

The patient tested negative for anti-ganglioside antibodies (GM1, GM2, GM3, GD1a, GD1b, GD3, GT1b, GQ1b, asialo GM1 (GA1), galactocerebroside (Gal-C)) and his cerebrospinal fluid protein amount (25 mg/dl) and cell count (0/μl) were normal. Brain MRI showed mild diffuse atrophy of the cerebellum. Spinal MRI revealed enlarged and gadolinium-enhanced nerve roots (figure 1E–J). Nerve conduction

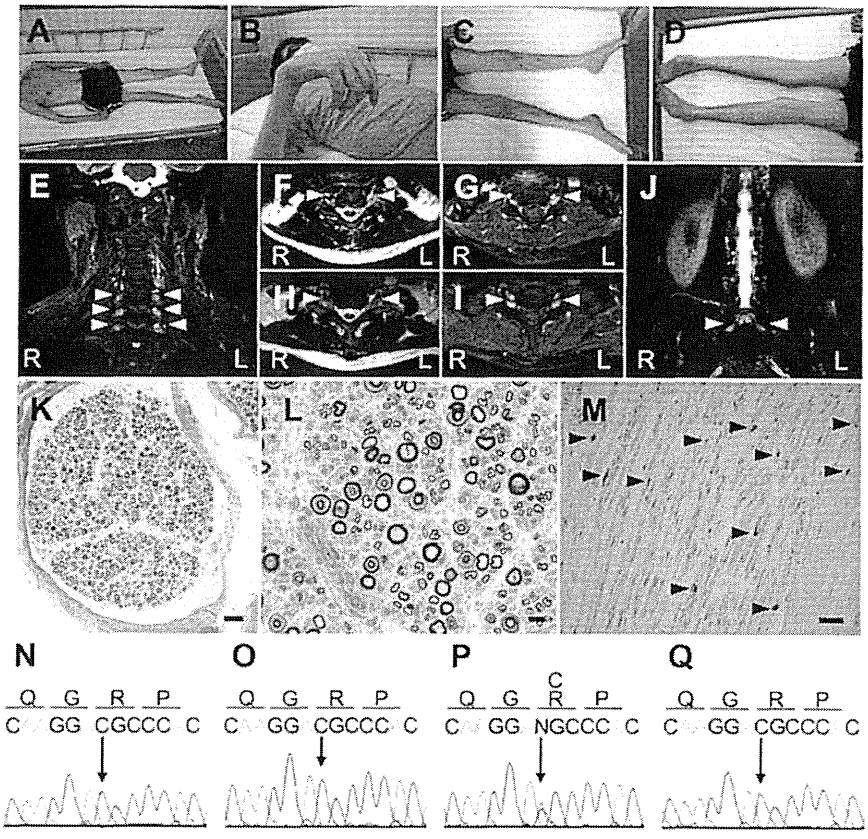

Figure 1 Clinical and pathological findings in a patient with amyotrophic lateral sclerosis 4 (ALS4). (A–D) Demographic features in a patient with ALS4. Long, thin limbs (A), right hand drop (B), bilateral pes cavus (C) and distal-dominant muscle atrophy of the lower extremities (D) are present. (E–J) MRI of the spinal cord. (E) T2-weighted image showing enlargement and T2 prolongation of the bilateral C6–8 nerve roots (arrowheads). (F, H) Axial T2-weighted MRI images showing enlargement and T2 prolongation of the C6 (F) and C7 (H) nerve roots (arrowheads). (G, I) Axial T1-weighted MRI images showing gadolinium-enhancement of the C6 (G) and C7 (I) nerve roots (arrowheads). (J) T2-weighted MRI image showing enlargement and T2 prolongation of the bilateral S1 nerve roots (arrowheads). (K–M) Pathology of the left sural nerve. (K, L) Toluidine blue staining showing moderate loss of myelinated fibres and thinly myelinated fibres (cross section). (M) Leucocyte common antigen (LCA) staining shows mild lymphocytic infiltration into the endoneurium (longitudinal section). (N–Q) Sequence electropherograms of the *senataxin* mutation. Normal and mutated DNA and amino acid sequences are shown. In the patient, a heterozygous C-to-T change at position 6406 (c. C6406T) in exon 19 results in an arginine to cysteine substitution (p. R2136C), as indicated by the arrow (P). The same heterozygous mutation is not detected in the father (N), mother (O) or sister (Q) of the patient. Scale bars =50 μm (K, M) and 10 μm (L). We were able to exclude IgM monoclonal gammopathy in the patient by demonstrating the absence of M-protein; sarcoidosis by demonstrating the absence of bilateral hilar lymphadenopathy and normal ACE level; paraneoplastic polyneuropathy by demonstrating normal tumour markers and a very long history of the illness since childhood; chronic inflammatory demyelinating polyradiculoneuropathy by demonstrating the presence of brisk tendon reflexes, ankle clonus, and dysuria and absence of multifocality and localisation of lesions in the biopsied sural nerve; multifocal motor neuropathy by demonstrating decreased sensory nerve conduction velocities and sensory nerve action potentials and the absence of anti-ganglioside antibodies; Sjögren syndrome by demonstrating the absence of anti-SS-A/SS-B antibodies; Charcot–Marie–Tooth disease by a genetic screening; hereditary spastic paraplegia by demonstrating the presence of sensory impairment and demyelinating neuropathy; and familial amyloidotic polyneuropathy by demonstrating the absence of amyloid deposits in the biopsied sural nerve.